

Identification of circular dorsal ruffles as signal platforms for the AKT pathway in glomerular podocytes

Rui Hua¹ | Jinzi Wei¹ | Mauricio Torres² | Yuxin He¹ | Yanan Li¹ |
 Xiaowei Sun¹ | Li Wang¹ | Ken Inoki^{2,3} | Sei Yoshida^{1,4} 

¹State Key Laboratory of Medicinal Chemical Biology, Frontiers Science Center for Cell Responses, College of Life Sciences, Nankai University, Tianjin, China

²Department of Molecular and Integrative Physiology, University of Michigan Medical School, Ann Arbor, Michigan, USA

³Internal medicine and Life Sciences Institute, University of Michigan, Ann Arbor, Michigan, USA

⁴Nankai International Advanced Research Institute, Shenzhen, China

Correspondence

Sei Yoshida, State Key Laboratory of Medicinal Chemical Biology, Frontiers Science Center for Cell Responses, College of Life Sciences, Nankai University, No. 94, Weijin Rd, Tianjin 300071, China.
 Email: seiyoshi@nankai.edu.cn

Funding information

Shenzhen Science and Technology Program; Frontiers Science Center for Cell Responses Grants from Nankai University

Abstract

Circular dorsal ruffles (CDRs) are rounded membrane ruffles induced by growth factors to function as precursors of the large-scale endocytosis called macropinocytosis. In addition to their role in cellular uptake, recent research using cell line systems has shown that CDRs/macropinocytosis regulate the canonical AKT-mTORC1 growth factor signaling pathway. However, as CDRs have not been observed in tissues, their physiological relevance has remained unclear. Here, utilizing ultrahigh-resolution scanning electron microscopy, we first report that CDRs are expressed in glomerular podocytes ex vivo and in vivo, and we visually captured the transformation process to macropinocytosis. Moreover, through biochemical and imaging analyses, we show that AKT phosphorylation localized to CDRs upstream of mTORC1 activation in podocyte cell lines and isolated glomeruli. These results demonstrate the physiological role of CDRs as signal platforms for the AKT-mTORC1 pathway in glomerular podocytes at the tissue level. As mTORC1 plays critical roles in podocyte metabolism, and aberrant activation of mTORC1 triggers podcytopathies, our results strongly suggest that targeting CDR formation could represent a potential therapeutic approach for these diseases.

KEY WORDS

AKT, circular dorsal ruffle, macropinocytosis, mTORC2, podocyte

1 | INTRODUCTION

Circular dorsal ruffles (CDRs) are crater-shaped membrane ruffles that appear on cell surfaces stimulated by growth factors, such as platelet-derived growth factor (PDGF), hepatocyte growth factor (HGF), insulin, and epidermal growth factor (EGF) (Hoon et al., 2012; Itoh & Hasegawa, 2013). The molecular mechanism and cellular functions of CDRs have been studied in the past decade (Hoon et al., 2012; Itoh & Hasegawa, 2013); our research group and others have found that CDRs transform into macropinocytosis, a large-scale solute uptake endocytosis, in fibroblasts and glioblastoma cells

(Bernitt et al., 2017; Dharmawardhane et al., 2000; Gu et al., 2011; Legg et al., 2007; Yoshida, Pacitto, Sesi, et al., 2018; Zdżalik-Bielecka et al., 2021). Live-cell imaging showed that after GF stimulation, membrane protrusions were evoked from the cell surface to become CDRs and they gradually shrunk towards the center of the structure and generated macropinosomes (Yoshida, Pacitto, Sesi, et al., 2018; Zdżalik-Bielecka et al., 2021).

GF stimulation activates several canonical signaling pathways, such as the cascade including phosphoinositide 3-kinase (PI3K), mechanistic target-of-rapamycin complex-2 (mTORC2), AKT, and mechanistic target-of-rapamycin complex-1 (mTORC1) (Fu &

Rui Hua and Jinzi Wei contributed equally to this study are the co-first authors.

Hall, 2020; Hoxhaj & Manning, 2020; G. Y. Liu & Sabatini, 2020; Yoshida, Pacitto, Inoki, et al., 2018). After GF stimulation, PI3K is activated and generates phosphatidylinositol (3,4,5)-triphosphate (PIP3) at the plasma membrane (Thorpe et al., 2015). The protein kinase AKT contains a pleckstrin homology (PH) domain that interacts with PIP3 (Manning & Toker, 2017; Várnai et al., 1999). Thus, once PIP3 is generated, AKT is recruited to the plasma membrane, where the protein is phosphorylated and activated by two distinct kinases, PDK1 and mTORC2 (Manning & Toker, 2017). Phospho-AKT functions upstream of mTORC1, which has a key role in cell growth and differentiation.

Recent studies have shown that CDR and macropinocytosis modulate the AKT/mTORC1 signaling pathway (Buckley & King, 2017; Stow et al., 2020; Swanson & Yoshida, 2019; Yoshida, Pacitto, Inoki, et al., 2018). Imaging analysis showed that PIP3 accumulates at macropinocytic cups in macrophages, resulting in the local recruitment of AKT (Pacitto et al., 2017; Wall et al., 2017; Yoshida et al., 2009). The inhibition of macropinocytosis was found to block AKT phosphorylation (pAKT) and mTORC1 activation in macrophages (Pacitto et al., 2017; Yoshida et al., 2015). A number of studies have shown that the expression of oncogenic Ras induces both macropinocytosis and mTORC1 activation (Bar-Sagi & Feramisco, 1986; Egami et al., 2014; Inoki et al., 2003; Mendoza et al., 2011). 5-(N-Ethyl-N-isopropyl)-amiloride (EIPA), which inhibits the small GTPase Rac1 function via lowering pH close to the plasma membrane, has been used to inhibit macropinocytosis in vitro and in vivo (Commissio et al., 2013; Koivusalo et al., 2010; Swanson & Watts, 1995; West et al., 1989). It is shown that EIPA diminished Ras-induced mTORC1 activation (Palm et al., 2015). NUMB protein negatively regulates CDR formation; depletion of NUMB increases HGF-induced pAKT (Zobel et al., 2018). Moreover, we recently described PIP3 generation and AKT recruitment to CDRs, and inhibition of CDR formation was shown to attenuate EGF-induced pAKT (Sun et al., 2022; Yoshida, Pacitto, Sesi, et al., 2018).

Podocytes are highly differentiated renal epithelial cells that cover the glomerular capillaries as an essential component of the kidney filtration barrier (Assady et al., 2017; Garg, 2018; Kopp et al., 2020), and CDR formation and macropinocytosis have been shown to occur in these cells (Bollée et al., 2011; Chung et al., 2015; Schell et al., 2013). Heparin-binding EGF-like growth factor (HB-EGF) was shown to induce CDR formation in cultured mouse podocytes (Bollée et al., 2011). EGF treatment generates CDRs in primary cultured podocytes (Schell et al., 2013). Staining of mouse tissue revealed that podocytes have active macropinosomes in vivo (Chung et al., 2015). However, the cellular function of CDRs and the interaction between CDRs and macropinocytosis in podocytes remain unclear, and microscopic detection of CDRs in vivo has not been reported. Thus, the physiological relevance of CDRs in podocytes should be investigated in vivo as well as ex vivo.

We hypothesized that podocyte CDRs precede macropinocytosis and regulate the AKT/mTORC1 pathway to maintain cell metabolism as a critical part of kidney function. In the current study, we tested this idea using different techniques to identify CDRs on podocytes in

vivo and ex vivo and investigated their role in the GF-induced AKT/mTORC1 pathway. High-resolution scanning electron microscopy (SEM) of mouse kidney tissue showed that glomerular podocytes displayed CDR-like structures in vivo. Moreover, both EGF and PDGF induced CDRs in the mouse podocyte cell line, MPC5. Inhibition of CDR formation significantly mitigated GF-induced pAKT and attenuated mTORC1 activation in cells. Confocal microscopy showed that PI3K/mTORC2/AKT signaling components localized to GF-induced CDRs. Importantly, we utilized isolated mouse glomeruli for ex vivo experiments and found that glomerular podocytes express CDRs as macropinocytic cups, regulating the AKT pathway. Thus, with these results, we have named the cellular function of CDRs ex vivo and in vivo, and we propose that CDRs are signaling platforms for growth factor-induced AKT pathways in podocytes as a critical part of the kidney filtration function.

2 | MATERIALS AND METHODS

2.1 | Reagents, plasmids, and antibodies

Recombinant murine EGF (315-09), murine PDGF-BB (315-18), and murine interferon- γ (IFN- γ) (315-05) were obtained from Peprotech. EIPA (1154-25-2) was obtained from Tocris. MK2206 (A3010) was purchased from APExBio. Wiskostatin was from Abcam (ab141085). The protease inhibitor cocktail (04693159001) was purchased from Roche. Collagen type I solution from rat tail (C3867-1VL) and collagenase (C9263) were purchased from Sigma-Aldrich. Paraformaldehyde (PFA; 16%, 28908) was from Thermo Fisher Scientific. Glutaric dialdehyde (25%, 16220) was from Electron Microscopy Sciences and Roswell Park Memorial Institute (RPMI)-1640 medium (C11975500BT), Opti-medium (Gibco, 31985-070), low-glucose Dulbecco's modified Eagle's medium (DMEM) (C11885500BT), Hank's balanced salt solution (HBSS) (14025-092), HBSS without magnesium and calcium (14175-079), and fetal bovine serum (10099141C) were obtained from Gibco. Dulbecco's phosphate-buffered saline (DPBS) (B220KJ) was purchased from Basalmedia. The antimycoplasmal drug plasmocin prophylactic was purchased from InvivoGen. Penicillin G Na salt (S17030) was purchased from Shanghai YuanyeBio-Technology. Streptomycin sulfate (A610494) was obtained from Sangon Biotech. Lipofectamine 2000 reagent (11668-019) was purchased from Invitrogen. Rhodamine phalloidin (RM02835) was obtained from ABclonal. The mounting medium with 4',6-diamidino-2-phenylindole (DAPI) (ab104139) was from Abcam. The AKT-GFP plasmid (#86637), mSin1-GFP plasmid (#72907), and Btk-PH-GFP plasmid (#51463) were purchased from Addgene. Cell strainers of 100 (15-1100), 70 (15-1070), and 40 μ m (15-1040) were obtained from Biologix. Fluorescein isothiocyanate-labeled dextran with an average molecular weight of 70,000 (FDx70) (D1823) was obtained from Invitrogen. Lucifer yellow (LY) (abs47048137) was obtained from Absin. The following materials were used for the immunofluorescence staining assays: WT1 (ABclonal; A17006, 1:50), Rab5a (CST; #21433, 1:50), SH3YL1 (Abcam; ab154123, 1:50),

cortactin (ABclonal; A9518, 1:50), p110 α (ABclonal; A0265, 1:50), p110 β (ABclonal; A0982, 1:50), AKT (CST; #9272 and #2920, 1:50), pAKT (CST; #4060, 1:50), mTOR (CST; #2983, 1:50), rictor (Proteintech; 27248-1-AP, 1:50), LAMP (Proteintech; 65050-1-Ig, 1:50), N-WASP (ABclonal; A2576, 1:50), nephrin (Abcam; ab216341, 1:50), synaptopodin (Proteintech; 21064-1-AP, 1:50), goat anti-rabbit IgG H&L Alexa FluorR 488 (Abcam; ab150081, 1:500), and goat anti-mouse IgG (H+L) Alexa Fluor 546 (Invitrogen; A-11030, 1:500). The western blot analysis materials were: AKT (CST; #9272, 1:2000), phospho-AKT (Ser473) (CST; #4060, 1:1000), MAPK (ERK1/2) (CST; #4695, 1:2000), phospho-MAPK (ERK1/2) (CST; #4376, 1:1000), S6K (CST; #2708, 1:2000), phospho-S6K (The389) (CST; #9234, 1:1000), and HRP-conjugated anti-rabbit IgG (GE Healthcare; NA934V, 1:5000).

2.2 | Cell culture and inhibitor treatments

The mouse podocyte cell line, MPC5, was obtained from Tongpai Biotechnology. The cells were cultured in RPMI-1640 medium containing recombinant murine IFN- γ (50 U/mL), 10% fetal bovine serum (FBS), and 1% penicillin-streptomycin at 33°C as described previously (Mundel et al., 1997). Differentiation was achieved by culturing the cells for 14 days at 37°C in RPMI-1640 with 10% FBS and antibiotics. Plasmocin prophylaxis was added at a ratio of 1:1000 to prevent mycoplasma contamination. All experiments were performed using Day 14 podocytes. Inhibitor treatments included EIPA (75 μ M), MK2206 (2 μ M), and wiskostatin (10 μ M). All inhibitors were applied for 30 min pretreatment in low-glucose DMEM at the concentrations described above. For amino acid starvation, HBSS (with magnesium and calcium) was added for 30 min after extracting the low-glucose DMEM.

2.3 | SEM

SEM samples of mouse glomeruli were prepared as previously described (Yoshida et al., 2021). Briefly, after mice were anesthetized and perfused with PBS followed by fixation buffer (2.5% glutaraldehyde, 2% formaldehyde in 0.1 M cacodylate buffer), the kidneys were dissected, incubated in fixation buffer for 1 h at 25 ± 2°C, and then stored at 4°C. Samples were submitted and processed for SEM by the University of Michigan Microscope and Image Analysis Core Facility using standard procedures (Yoshida et al., 2021). For advanced SEM observations, we used the Thermo Fisher Helios 650 Nanolab SEM at the Michigan Center for Materials Characterization. SEM samples of the MPC5 cells were prepared as follows: cells were prepared on 17-mm collagen-coated coverslips, incubated in low glucose DMEM without FBS for 18 h, stimulated by 16 nM EGF or 2 nM PDGF for 5 min, and then fixed using 2.5% glutaraldehyde (in Sorensen buffer, 35.76 g Na₂HPO₄ and 9.08 g KH₂PO₄ in 1 L ddH₂O, pH = 7.2) at 4°C overnight. The samples were then dehydrated and embedded in Yimingfuxing Bio.

A field emission SEM (FEI Apreo S LoVac) was used at the Central Laboratory of Nankai University to examine the CDR structures in the podocytes.

2.4 | Immunofluorescence staining and confocal microscopy

After starvation and stimulation, the cells were fixed on 17-mm coverslips with 4% PFA in PBS buffer for 30 min and then washed in TBST (Tris 200 mmol/L, NaCl 3 mol/L, pH = 7.4). After washing, the cells were permeabilized in 0.1% Triton X-100 for 5 min, blocked in 5% bovine serum albumin (BSA) (in TBST) for 30 min, and then washed at 25 ± 2°C. Primary antibodies were diluted in 5% BSA and cells were incubated in antibody solution at 4°C overnight. Secondary antibodies were diluted in 5% BSA and the cells were incubated for 2 h at 25 ± 2°C. Rhodamine phalloidin was diluted as 1:100 in 5% BSA to mark actin, and the cells were incubated for 1 h at 25 ± 2°C. Coverslips were mounted using a mounting medium with DAPI at 25 ± 2°C. The samples were examined using a Leica TCS SP5 confocal microscope at the Core Facility of the College of Life Sciences of Nankai University.

2.5 | Macropinosome assay in vitro

Cells were cultured overnight on coverslips in low-glucose DMEM without FBS. PDGF (2 nM) or EGF (16 nM) were added together with fluorescein dextran (FDx70; 0.5 mg/mL), and the cells were incubated at 37°C for 5 or 30 min. Cells were fixed with 4% PFA in PBS at 37°C for 30 min. The fixed cells were washed three times with DPBS for 10 min at 25 ± 2°C and mounted. Fifteen phase-contrast and FITC-FDx70 images of each sample were taken using a Live Cell Station (Zeiss Axio Observer Z1) at the Core Facility of the College of Life Sciences of Nankai University. The number of induced CDRs was counted using phase-contrast images and the number of induced macropinosomes was determined by counting FDx70-positive vesicles. More than 5000 cells were counted from each sample.

2.6 | Cell lysates and western blot analysis

Cells were stimulated with EGF/PDGF (with varied duration) and then lysed for 10 min in cold lysis buffer (40 mM HEPES pH 7.5, 120 mM NaCl, 1 mM EDTA, 10 mM pyrophosphate, 10 mM glycerophosphate, 1.5 mM Na₃VO₄, 0.3% CHAPS, and a mixture of protease inhibitors). Lysates were centrifuged at 13,000g for 15 min at 4°C. The supernatant was mixed with 5× sodium dodecyl sulfate (SDS) sample buffer and boiled for 5 min. The samples were subjected to SDS-polyacrylamide gel electrophoresis (SDS-PAGE) and western blot analysis with the indicated antibodies, as described previously.

2.7 | CDR assay

The same fixative used for coverslips for immunofluorescence staining was used for the CDR assay. Samples were stained with rhodamine phalloidin and mounting medium with DAPI to count the CDRs and cells. A ZEISS Axio Imager Z1 at the Core Facility of the College of Life Sciences of Nankai University was used to obtain images under a magnification of $\times 20$. Fifteen images were randomly taken from each sample, and more than 2000 cells were counted per condition. The CDR frequency was calculated as the number of cells showing CDRs in proportion to the total number of cells counted, and the CDR frequency was compared between the inhibitor-treated group and the control group. The average and standard error of the ratios were calculated from at least three independent experiments using a two-tailed Student's *t*-test.

2.8 | Quantification of signal intensity at CDRs

Images were analyzed using ImageJ. Original images were opened and converted to 8-bit images for quantification. pAKT (or rictor) image was used to generate the THRESHOLD image, which determines the pAKT (or rictor) signal positive area, and saved as "Image 1." Next, pAKT/AKT (or rictor/AKT) RATIO images were prepared and saved as "Image 2." "Image 1" and "Image 2" were combined to generate the AND image, which shows the ratio value only on the signal positive area, and this image was saved as "Image 3." CDR areas on "Image 3" were measured, and the average of the ratio value inside each area was measured.

2.9 | Plasmids transfection

The Btk-PH-GFP, AKT-GFP, and mSin1-GFP plasmids were purified using an EndoFree Midi Plasmid Kit (TIANGEN; #DP108). A plasmid volume of 0.4 μ g was applied to each coverslip in the transfection step. A volume of 50 μ L Opti-medium with plasmid was added to 50 μ L Opti-medium with 2 μ L Lipofectamine 2000 reagent. The mixed Opti-medium was added to 500 μ L RPMI-1640 (with FBS, antibiotics, and antimycoplasma drugs) for each sample. After 6 h, the medium was replaced with fresh RPMI-1640 medium for 4 h and then changed to low-glucose DMEM for 18 h of starvation. GF treatments, fixation procedures, and observations were carried out as described above in Section 2.4.

2.10 | Isolation of glomeruli

Isolated mouse glomeruli were prepared as previously described (Wang et al., 2019). Adult C57BL/6N mice, 8–10 weeks of age, were used in this study. After the mice were anesthetized and killed, the kidneys were carefully removed from each animal, and a few drops of HBSS were applied to avoid drying. None of the HBSS used in the

isolation procedure contained any magnesium or calcium. Renal cortices were minced into tiny particles (approximately 1 mm³) with a blade and then transferred to 1.5-mL tubes containing 500 μ L HBSS. The mixture was centrifuged at 210g for 5 min, after which the particles were transferred to 5 mL collagenase (1 mg/mL in HBSS) to digest for 15 min in a water bath at 37°C. The resulting liquid was then gently pipetted 20 times at 5-min intervals. The digestion was stopped by adding 5 mL RPMI-1640 medium supplemented with 10% FBS, and the mixture was centrifuged at 210g for 5 min. The pellet was resuspended in 5 mL cold HBSS. The resulting mixture was transferred to a 100- μ m cell strainer. The large particles were pressed through a 100- μ m cell strainer using the rubber plunger of a 1-mL syringe. The filtrate was collected and washed, first through a 70- μ m cell strainer and then a 40- μ m cell strainer. The fragments that remained on the 40- μ m strainer were rinsed with cold HBSS and transferred to a clean cell culture dish. After 2 min of settling, the supernatant was collected and washed through another 40- μ m cell strainer. The fragments that remained on this strainer were rinsed with cold HBSS and transferred to another clean cell culture dish. The supernatant was collected and, after 2 min of settling, 0.01% (w/v) polyvinylpyrrolidone (PVP) was added and the mixture was centrifuged at 210g for 5 min to collect the glomeruli.

2.11 | SEM and immunofluorescence staining of isolated glomeruli

After isolation, glomeruli SEM samples were directly fixed with 2.5% glutaraldehyde in the Sorensen buffer, as described previously. The samples were sent to Yimingfuxing Bio for dehydration and examined using a field emission SEM (FEI Apreo S LoVac) at the Central Laboratory of Nankai University. For immunofluorescence staining of glomeruli, 4% PFA in PBS was used for fixation at 25 ± 2°C for 1 h. For permeabilization of isolated glomeruli, 0.1% Triton X-100 was used for 10 min with gentle rotation, followed by a 30-min blocking period with 5% BSA. Primary antibodies and rhodamine phalloidin (1:50) were mixed with 5% BSA for 3 h treatment with gentle rotation. Samples were treated with secondary antibodies (1:200) for 2 h and then DAPI solution (in 5% BSA, 1:2000) for 10 min. The samples were washed with TBST (5 min × 3) between each step and then mounted in 35% glycerol in TBST. At the end of each step, the mixture was centrifuged (3 min, 210g), and the glomerular pellets were collected. A Leica TCS SP5 confocal microscope was used at the Core Facility of the College of Life Sciences of Nankai University to examine the samples. For each glomerulus, 20–21 images were taken from the top, with a 0.76- μ m interval between each image. EIPA (40 μ M) was applied before the addition of EGF (80 nM, 15 min) to HBSS.

2.12 | Projection assay

Isolated glomeruli were treated with LY (0.5 mg/mL) for 5 or 30 min at 37°C. After washing three times with PBS containing PVP, the

glomeruli were fixed in 4% PFA in PBS at $25 \pm 2^\circ\text{C}$ for 1 h. Immunofluorescence (IF) staining of actin and pAKT was performed as described above. The XY-projection images were constructed from confocal scanning images taken from the top 15 μm of each glomerulus, and the total signal intensities were measured. Projection images of the actin staining were used to identify the shape of each glomerulus, and the average intensity of the target signal was calculated as (total intensity per glomerulus)/(area of each glomerulus).

2.13 | Preparation of isolated glomerulus lysates

Isolated glomeruli were treated with dimethylsulfoxide or EIPA (75 μM , 30 min), stimulated with EGF (80 nM, 15 min), and then lysed using cold lysis buffer (40 mM HEPES, 120 mM NaCl, 1 mM EDTA, 10 mM pyrophosphate, 10 mM glycerophosphate, 1.5 mM sodium vanadate, and 0.3% CHAPS, pH = 7.5). The lysates were then subjected to SDS-PAGE and western blot analysis with the indicated antibodies, as described in Section 2.6.

2.14 | Statistical analysis

All experiments were conducted at least twice or with at least two biological replicates. Results are expressed as mean \pm SEM. *p* Values of less than 0.05 were considered statistically significant. Two-tailed paired Student's *t*-test was used for comparisons between two groups in Figure 4*h* (*n* = 5); Figure 4*j* (*n* = 5); Supporting Information: Figure S3 (*n* = 3); Supporting Information: Figure S4*d,e* (*n* = 5); and Supporting Information: Figure S4*h,i* (*n* = 3). Two-tailed unpaired Student's *t*-test was used for comparisons between the two groups in Figure 5*j,k* (*n* > 12); Figure 6*c* (*n* > 40); Figure 7*b* (*n* > 16); Figure 7*e* (*n* = 26); Figure 7*g* (*n* = 6); Figure 7*h* (*n* = 3); and Supporting Information: Figure S6*g,h* (*n* > 12).

3 | RESULTS

3.1 | Glomerular podocytes express CDRs as precursors of macropinocytosis

Ultrahigh-resolution SEM of mouse glomeruli was used to further characterize the morphology of podocytes. Unexpectedly, we found crater-shaped membrane ruffles on the surfaces of glomeruli (Figure 1, arrows). Higher-magnification images show rounded membrane ruffles (Figure 1, enlarged images) protruding from the podocyte cell body, which is the center of podocytes, and an elongated unique cellular structure called the primary/foot process. We identified a total of 21 glomeruli from five mice and found that 25.38% of 528 podocytes induced the rounded membrane ruffles.

Membrane ruffles can be induced by growth factors (Hoon et al., 2012; Itoh & Hasegawa, 2013; Kay, 2021; Swanson, 2008).

Thus, we analyzed the EGF-stimulated mouse podocyte cell line, MPC5. Actin was stained to identify CDRs (Hoon et al., 2012; Itoh & Hasegawa, 2013; Sun et al., 2022), and antibodies against WT1 were used as a marker of podocytes (Guo et al., 2002; Inoki et al., 2011; Yoshida et al., 2021). The results showed that actin formed ring structures covering the central part of the cells (Figure 2*a*, EGF, arrows), suggesting that EGF induced CDRs in these cells. Quantification analysis from 30 independent experiments confirmed that EGF induced CDRs in MPC5 at an efficiency of 30.17% in 63,606 cells analyzed. We also found that PDGF induced CDRs in MPC5 (10.91% of 65,287 cells from 30 independent experiments) (Figure 2*a*, PDGF, arrows). Interestingly, podocytes also induced CDRs—although rarely—under culture conditions (Figure 2*a*, culture condition, arrow). Recruitment of Rab5a (Lanzetti et al., 2004; Palamidessi et al., 2008), SH3YL1 (Hasegawa et al., 2011), and cortactin (Cortesio et al., 2010) were used as the CDR marker (Sun et al., 2022). We also found that these proteins were expressed at GF-induced CDRs (Figure 2*b-d*). Thus, we concluded that GF treatment induces CDRs in podocytes.

The results also revealed different sizes of CDRs in the cells after stimulation (Figure 2*a*, arrows), suggesting that CDRs shrink to the center and form macropinosomes, as observed in mouse embryonic fibroblasts (MEFs) (Yoshida, Pacitto, Sesi, et al., 2018). Ultrahigh-resolution SEM was used to depict the structure of the CDRs in MPC5. It clearly showed that cup-like structures were evoked as CDRs from the cell surfaces (Figure 3*a,b* and Supporting Information: Figure S1*a,b*). We identified at least four different morphological steps: (1) circular protrusions were evoked from the surface of the cell, (2) the structure was elongated in the vertical direction to form wall-like membrane ruffles, (3) the membrane ruffles were waved and bent to the inside at the edge, and (4) the top open area was closed by a fusion of the ruffles (Figure 3*c,d* and Supporting Information: Figure S1*c,d*), suggesting that the CDR functions as macropinocytic cups. To evaluate the ingestion activity of CDR via macropinocytosis, we used FDx70 as a probe for the ingestion of extracellular solutes. Phase-contrast images clearly showed CDR structures 5 min after EGF stimulation (Figure 3*e*, arrows) and FDx70 fluorescence appeared as circular structures in the cells after 30 min (Figure 3*e*, arrowheads). In fact, the time-course experiment revealed that, whereas the number of induced CDRs decreased, the signal intensity of FDx70 increased during the observation period (Figure 3*f,g*), suggesting that the CDRs changed to macropinosomes and ingested FDx70. These data indicate that GF-induced CDRs form macropinosomes in podocytes, which ingest extracellular solutes.

3.2 | CDRs are required for the AKT-mTORC1 pathway in podocytes

EGF and PDGF activate the AKT/mTORC1 pathway in different cell lines (Chen et al., 2016; Hoxhaj & Manning, 2020; Ying et al., 2017). Accordingly, we confirmed that GF-induced pAKT in MPC5 within 1 min of stimulation (Supporting Information:

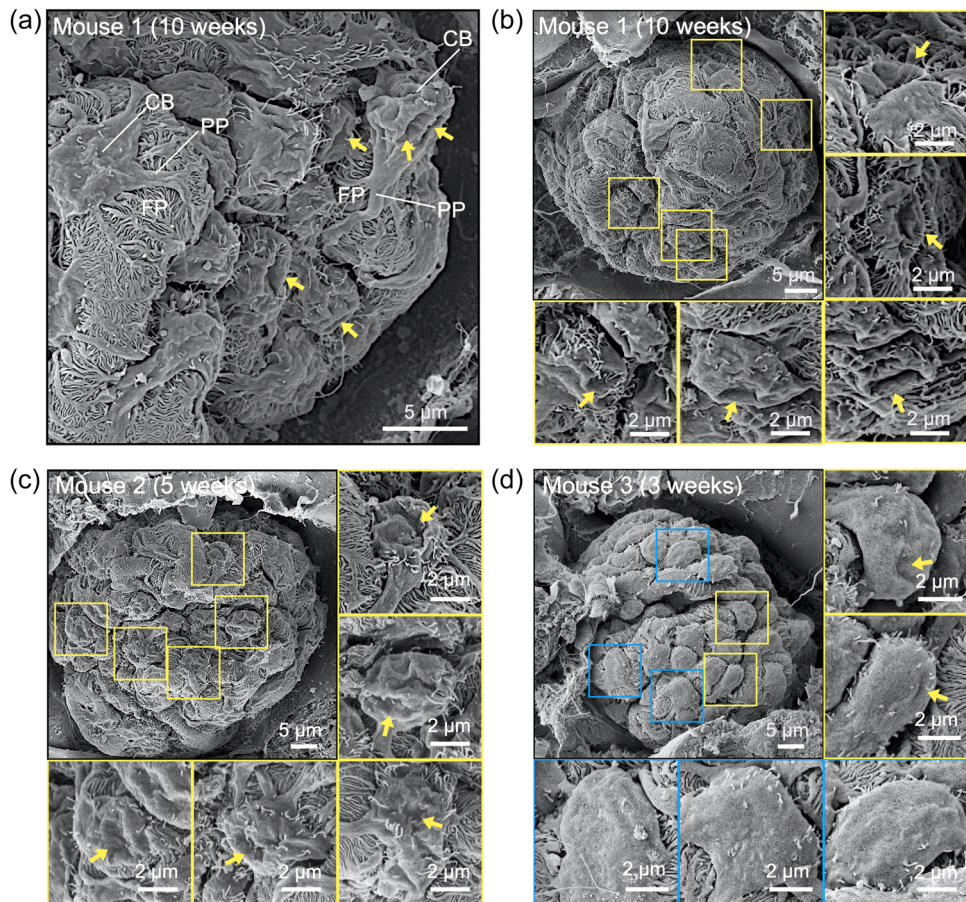


FIGURE 1 Representative high-resolution scanning electron microscopy (SEM) images of mouse glomeruli showing circular dorsal ruffle (CDR)-like structures in podocytes. The arrows indicate CDR-like structures; the squares indicate podocytes with (yellow) or without (blue) CDR-like structures. In total, 21 glomeruli from five mice were examined using SEM. The glomeruli were from mice aged 10 weeks (a and b) ($n = 8$ glomeruli from one mouse), 5 weeks (c) ($n = 14$ glomeruli from two mice), and 3 weeks (d) ($n = 3$ glomeruli from two mice). CDR-like structures formed in 25.38% of the podocytes ($n = 528$). Scale bars: 5 and 2 μ m. CB, the cell body of podocytes; PP, primary process; FP, foot process.

Figure S2a,b). As an output of mTORC1 activation, pS6K was also evident. Following stimulation with both EGF and PDGF, pS6K expression was induced for 5 min (Supporting Information: Figure S2a,b), thus supporting the established model that AKT acts upstream of mTORC1. ERK phosphorylation, another downstream signaling molecule of GF stimulation, was observed at 1 min (Supporting Information: Figure S2a,b). To test the role of CDRs in growth factor signaling, we used EIPA, which has been used as a macropinocytosis inhibitor in vitro and in vivo (Commissio et al., 2013; Koivusalo et al., 2010; Swanson & Watts, 1995; West et al., 1989). EIPA treatment diminished GF-induced pAKT and pS6K (Figure 4a,b and Supporting Information: Figure S3a,b) and completely blocked GF-induced CDR formation (Figure 4g-j), suggesting that CDRs are required for the AKT/mTORC1 pathway. The actin polymerization protein N-WASP has been observed at CDRs, and the N-WASP inhibitor, wiskostatin, is known to block CDRs (Legg et al., 2007; Schell et al., 2013). To confirm the role of CDRs in the AKT/mTORC1 pathway and exclude the possibility of side effects of EIPA treatment, we also used wiskostatin. Confocal microscopy showed that N-WASP was

located at CDRs (Supporting Information: Figure S4a) and that wiskostatin blocked GF-induced CDRs in MPC5 cells (Supporting Information: Figure S4b-e). Biochemical analysis showed that wiskostatin treatment blocked GF-induced pAKT and pS6K (Supporting Information: Figure S4f-i). These results strongly suggest that CDRs regulate the AKT/mTORC1 pathway.

When we used the AKT-specific inhibitor MK2206, we found that, although pAKT was completely blocked (Figure 4c,d and Supporting Information: Figure S3c,d), CDRs were still induced by GFs (Figure 4g-j). Thus, AKT was not upstream of CDR formation. It has been shown that extracellular amino acids ingested by macropinocytosis activate mTORC1 in growth factor signaling (Yoshida et al., 2015). We found that GF treatment-induced pAKT, but not pS6K, under amino acid starvation conditions (Figure 4e,f and Supporting Information: Figure S3e,f), suggesting that ingestion of extracellular amino acids is necessary for mTORC1 activation in podocytes. Based on these results, we concluded that CDRs in podocytes work upstream of the GF-induced AKT/mTORC1 pathway via two mechanisms: (1) CDRs function as a signaling platform for AKT activation and (2) CDR

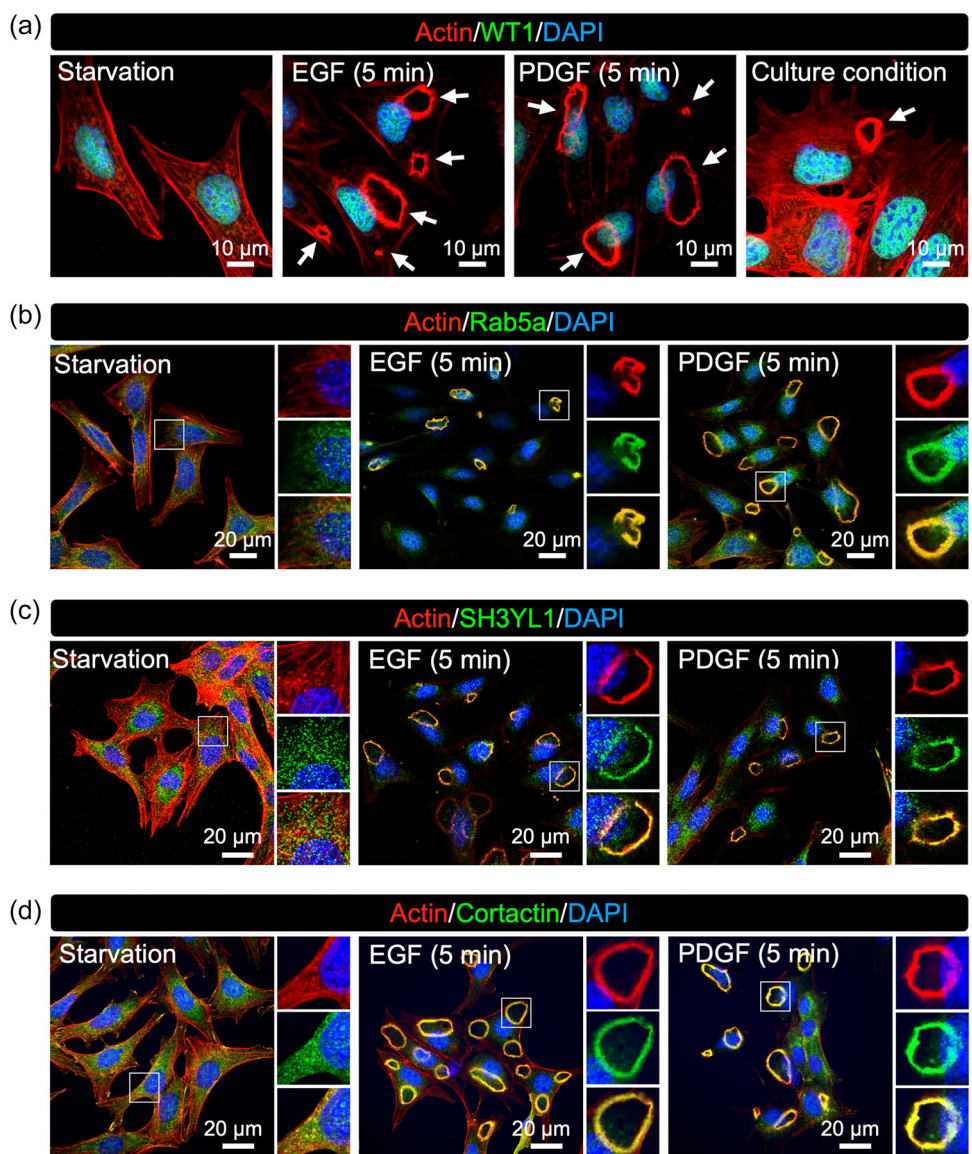


FIGURE 2 Epidermal growth factor (EGF) and platelet-derived growth factor (PDGF) induce circular dorsal ruffle (CDRs) in the mouse podocyte cell line MPC5. (a) Representative confocal images of growth factor (GF)-treated MPC5 cells. Treatment with EGF and PDGF for 5 min induced CDR formation (white arrows), identified by actin staining (red). Podocytes also induced CDRs under culture conditions (Culture condition). The transcription factor WT1 (green) was used as a podocyte marker. $n = 6, 6, 6$, and 11 images from left to right. (b–d) Representative confocal images of actin (red) with Rab5a (green in b) ($n = 12, 17$, and 14 images from left to right), SH3YL1 (green in c) ($n = 8, 8$, and 8 images from left to right), or cortactin (green in d) ($n = 9, 8$, and 8 images from left to right) with and without GF stimulations. Rab5a, SH3YL1, and cortactin were used as CDR markers. Scale bars: $10\ \mu\text{m}$ (a) and $20\ \mu\text{m}$ (b–d). DAPI, 4',6-diamidino-2-phenylindole.

ingests extracellular nutrients via macropinocytosis to activate mTORC1.

3.3 | PI3K/mTORC2/AKT pathway is activated at CDRs

AKT and mTORC2 are recruited to the plasma membrane by interacting with PIP3, which is generated by PI3K (Fu & Hall, 2020; Hoxhaj & Manning, 2020; G. Y. Liu & Sabatini, 2020; Yoshida, Pacitto, Inoki, et al., 2018). Our confocal microscopy observations revealed

that the PI3K catalytic subunits p110 α (Figure 5a and Supporting Information: Figure S5a) and p110 β (Supporting Information: Figure S5b) isoforms were recruited to the CDRs. Thus, we tested whether PIP3 is generated at CDRs by utilizing GFP-tagged Btk-PH, an established probe protein to localize PIP3 (Várnai et al., 1999; Yoshida et al., 2009). Confocal microscopy showed strong GFP-Btk-PH signals at CDRs in GF-stimulated cells expressing probe proteins (Figure 5b and Supporting Information: Figure S5c). mSin1 is a key component of mTORC2 (Fu & Hall, 2020). We also utilized GFP-AKT and GFP-mSin1 and found that these proteins were recruited to CDRs (Supporting Information: Figure S5d,e). These results suggest

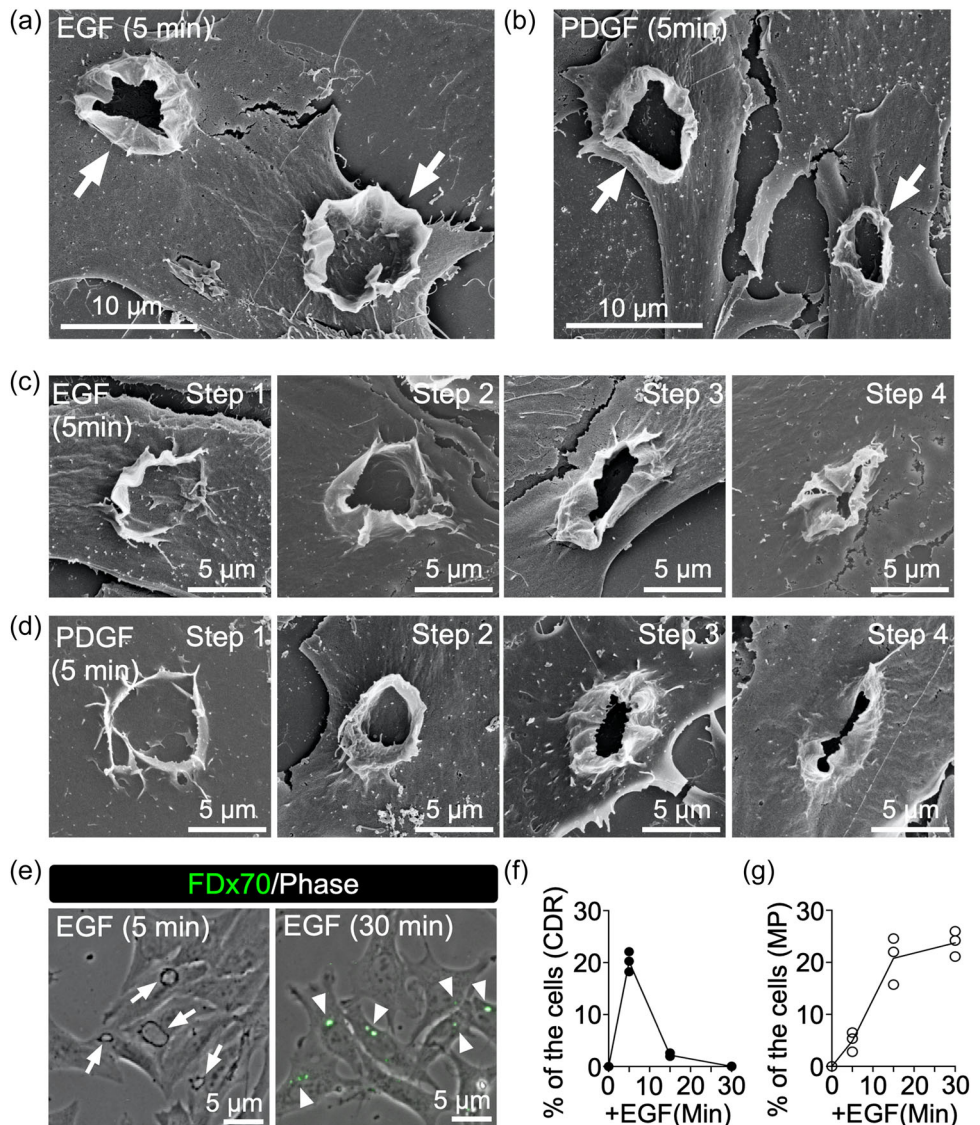


FIGURE 3 Circular dorsal ruffles (CDRs) function as macropinocytic cups in the mouse podocyte cell line MPC5. (a and b) Representative high-resolution scanning electron microscope (SEM) images of growth factor (GF)-induced CDRs in MPC5 cells. Treatment with epidermal growth factor (EGF) (a) and platelet-derived growth factor (PDGF) (b) for 5 min induced cup-like structures as CDRs (white arrows). $n = 22$ (a) and 28 (b) images. Additional images are shown in Supporting Information: Figure S1a,b. (c and d) Representative high-resolution SEM images of CDRs induced by EGF (c) or PDGF (d) showing four different morphological steps. $n = 4, 9, 7$, and 5 images (c) and 7, 9, 9, and 7 images (d) from left to right. Additional images are shown in Supporting Information: Figure S1c,d. (e) Imaging analysis identified CDRs (arrows in 5 min) and macropinosomes identified by FDx70 (green) (arrowheads in 30 min) in MPC5 cells after EGF treatment. $n = 45$ images each. (f and g) Quantification analysis from three independent time-course experiments revealed that while CDRs disappeared (f) macropinosomes were generated (g) during the imaging process. Scale bars: 10 μm (a and b) and 5 μm (c–e).

that CDRs are used as signaling platforms for the PI3K/mTORC2/AKT pathway.

To test whether AKT is phosphorylated by mTORC2 at CDRs, we performed several IF staining. Similar to the results of the over-expression experiment, the endogenous AKT was found to be localized at CDRs (Figure 5c and Supporting Information: Figure S6a). The staining patterns of AKT and pAKT (473) at CDRs completely matched (Figure 5d and Supporting Information: Figure S6b), suggesting that AKT is phosphorylated at the CDRs by mTORC2. Rictor and mTOR are components of mTORC2 (Fu &

Hall, 2020). The IF staining also revealed that both mTOR (Figure 5e and Supporting Information: Figure S6c), and rictor (Figure 5f and Supporting Information: Figure S6d) were localized at the CDRs. IF detection of LAMP, a marker of late endosomes, did not reveal the localization of LAMP to the CDR (Figure 5g), indicating that LAMP is useful as a negative control to ensure that IF staining identifies specific signals at CDRs.

Western blot analysis showed that the AKT inhibitor MK2206 completely blocked GF-induced pAKT (473) (Figure 4c,d and Supporting Information: Figure S3c,d). Accordingly, once we

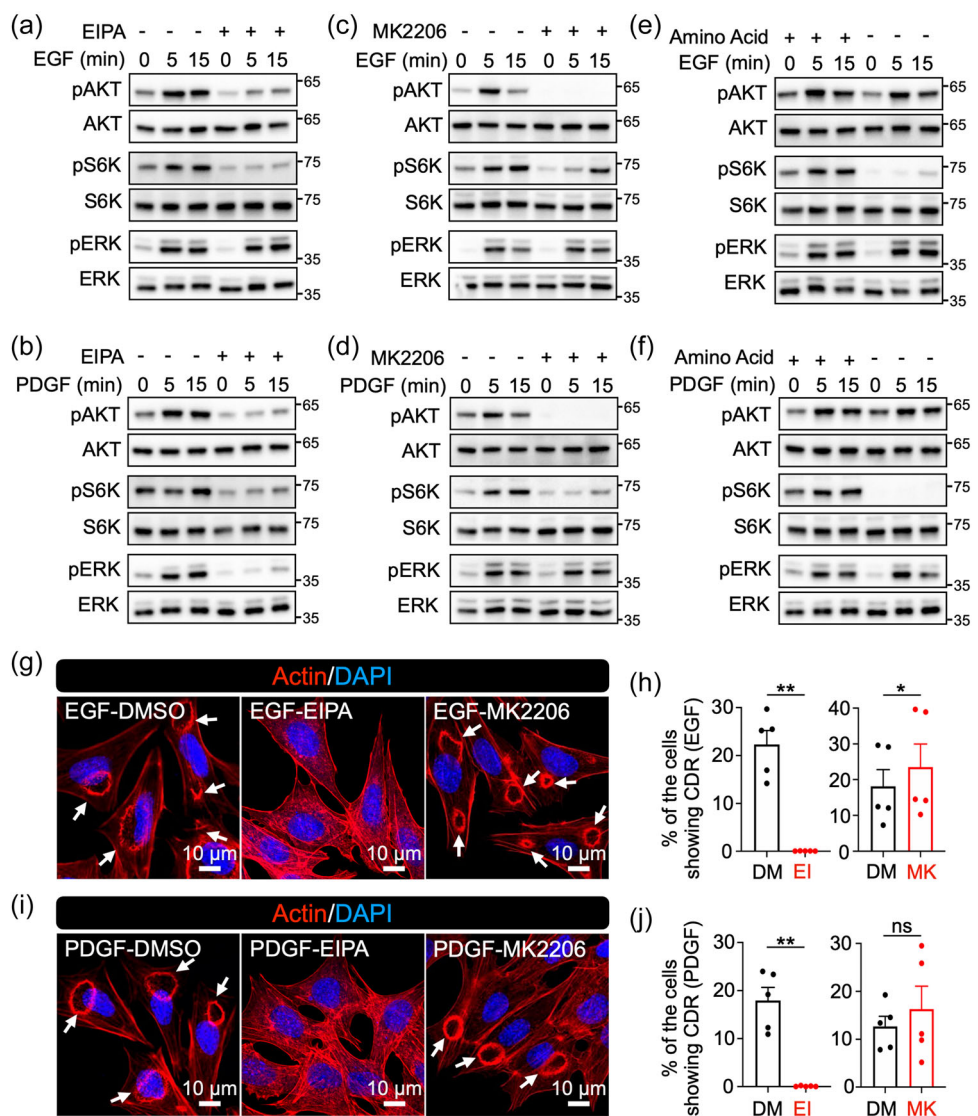


FIGURE 4 Circular dorsal ruffles (CDRs) regulate growth factor (GF)-induced AKT/mTORC1 signaling in MPC5 cells. (a and b) Inhibition of CDRs attenuated AKT phosphorylation (pAKT) and S6K phosphorylation (pS6K) levels. Western blot analysis of AKT, S6K, and ERK levels after epidermal growth factor (EGF) (a) or platelet-derived growth factor (PDGF) (b) stimulation with and without the macropinocytosis inhibitor 5-(N-Ethyl-N-isopropyl)-amiloride (EIPA). (c and d) Western blot analysis of AKT, S6K, and ERK levels after EGF (c) or PDGF (d) stimulation with and without the AKT inhibitor MK2206. (e and f) Western blot analysis of AKT, S6K, and ERK levels after EGF (e) or PDGF (f) stimulation with and without amino acids. Data are representative of at least three independent experiments (a–f). Quantification results are shown in Supporting Information: Figure S3. (g and i) Representative confocal images of MPC5 cells stimulated by EGF (g) ($n = 75$ images each) or PDGF (i) ($n = 75$ images each) with and without EIPA or MK2206. The arrows indicate CDRs. Scale bar: 10 μm. (h and j) The results of CDR assays from five independent experiments showed that EIPA treatment blocked GF-induced CDRs, but MK2206 did not. ** $p < 0.01$; * $p < 0.05$; ns, not significant. Two-tailed paired Student's *t*-test was used to compare the two groups. DMSO, dimethylsulfoxide.

treated cells with the AKT inhibitor, the signal intensity of pAKT (473) at CDRs was significantly weaker compared to no treatment, whereas the intensities of AKT at CDRs in both cases were similar (Figure 5h,j and Supporting Information: Figure S6e,g). In contrast, rictor was retained at the CDRs of the MK2206-treated cells (Figure 5i,k and Supporting Information: Figure S6f,h), supporting the hypothesis that pAKT(473) is induced by mTORC2 at CDRs. Thus, these results strongly suggest that PIP3 generated at the CDRs recruits both AKT and mTORC2, leading to CDR-dependent pAKT.

3.4 | Podocytes induce CDRs to modulate the AKT pathway at the surface of the isolated glomerulus

Although the results of our *in vivo* experiments clearly showed that glomerular podocytes induce CDRs (Figure 1), the limitations of this approach meant that we could not identify the particular cellular function. Cell line experiments indicated that CDRs regulate the AKT pathway in podocytes (Figures 2–5 and Supporting Information: Figures S1–6); however, the physiological relevance was not clear. To confirm these complementary results, we isolated mouse glomeruli

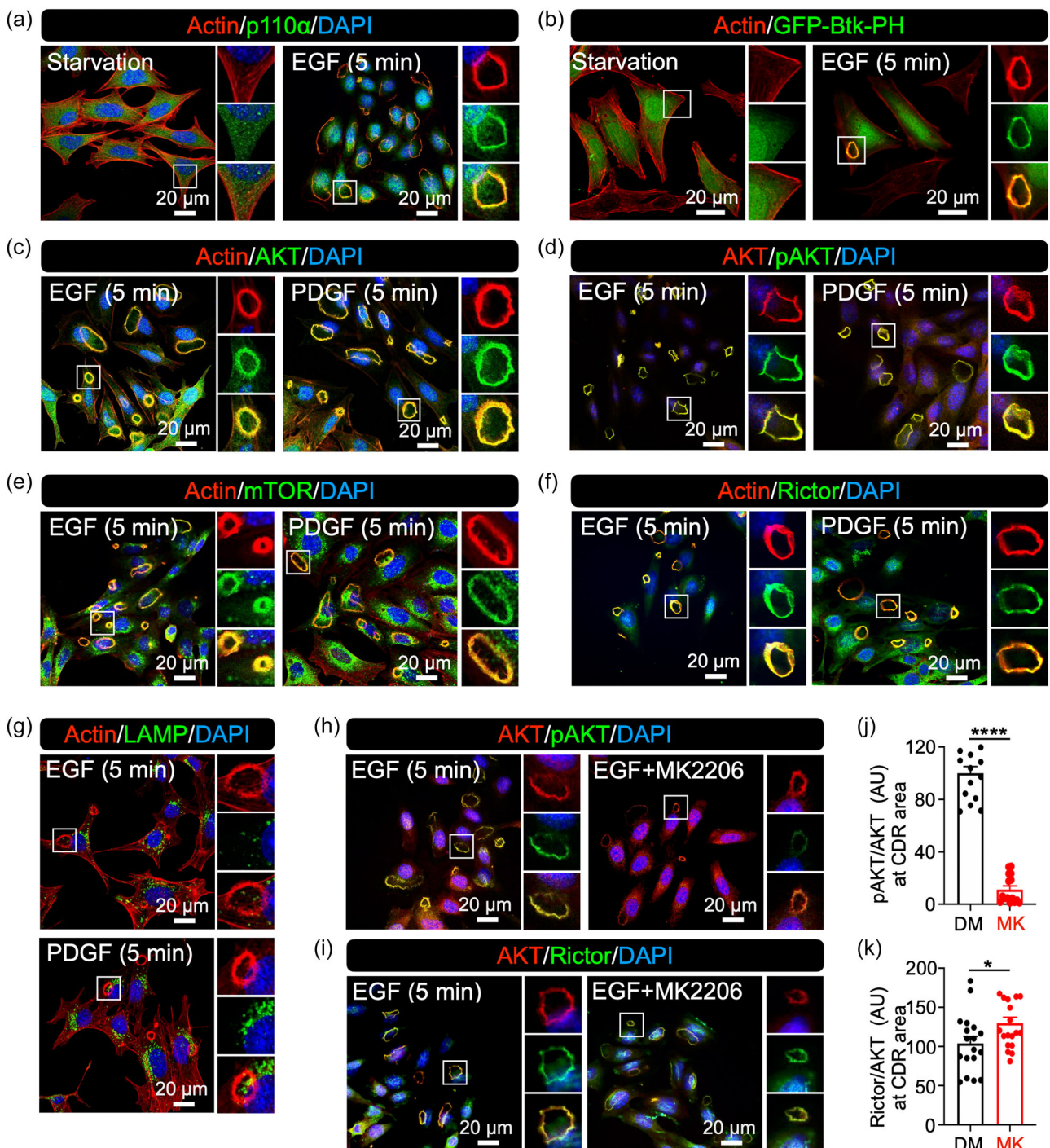


FIGURE 5 The PI3K/mTORC2/AKT signaling pathway is activated at circular dorsal ruffles (CDRs) in MPC5 cells. (a) Representative confocal images of actin (red)/p110 α (green) staining with and without epidermal growth factor (EGF) stimulation. $n = 10$ each. (b) Representative confocal images of actin (red) and GFP-Btk-PH (green) signal with and without EGF stimulation. $n = 11$ (left) and 16 (right). (c and d) Representative confocal images of actin (red)/AKT (green) staining (c) ($n = 10$ and 9, from left to right) and AKT (red)/pAKT (green) (d) ($n = 8$ and 6, from left to right) staining with EGF or platelet-derived growth factor (PDGF) stimulation. (e and f) Representative confocal image of actin (red)/mTOR (green) (e) ($n = 11$ and 10, from left to right) and actin (red)/rictor (green) (f) ($n = 20$ and 16, from left to right) staining with EGF or PDGF stimulation. (g) Representative confocal image of actin (red)/LAMP (green) in MPC5 after growth factor stimulations. LAMP, which was not located at the CDRs, was used as a negative control. $n = 11$ each. (h and i) Representative confocal images of AKT (red)/pAKT (green) (h) ($n = 22$ each) and AKT (red)/rictor (green) (i) ($n = 20$ each) staining after EGF stimulation with and without MK2206. (j and k) Quantification of the ratio of pAKT/AKT (j) and rictor/AKT (k) at CDRs. MK2206 treatment attenuated the signal intensity of pAKT, but not rictor, at CDRs after EGF stimulation with and without MK2206. More than 12 CDR images from two independent experiments were analyzed. **** $p < 0.0001$; * $p < 0.05$. A two-tailed unpaired Student's t-test was used for the statistical analysis. Scale bars: 20 μ m. AU, arbitrary unit; DAPI, 4',6-diamidino-2-phenylindole.

and performed ex vivo imaging and biochemical analyses. Mouse glomeruli were successfully isolated according to an established method (Wang et al., 2019), and the details of the surface structure were observed by ultrahigh-resolution SEM (Figure 6a). We observed that CDRs formed in podocytes on the surface of the glomerulus following EGF treatment (Figure 6a, squares). As in the case of the cell lines (Figure 3c,d and Supporting Information: Figure S1c,d), the closing process of the structure was visualized (Figure 6a, arrows). CDRs were occasionally observed on the surface of glomeruli, even without EGF treatment (Supporting Information: Figure S7a).

Using the ex vivo system, we carried out three-dimensional imaging to observe signals in podocytes on the surface of isolated glomeruli. SEM images revealed that the diameter of the podocytes was approximately 40 μm (Figure 6a and Supporting Information: Figure S7a). Thus, for IF observations of the upper half of the glomerulus, we scanned the structure every 0.76 μm along the z-axis from the top of the shape as +0 μm until the +15 μm section (Figure 6b). First, to test whether these CDRs precede macropinocytosis, we used the fluid-phase probe LY as a representative extracellular molecule (Berthiaume et al., 1995; Yoshida et al., 2015), and we monitored the LY signal inside the glomerular podocytes. Isolated glomeruli were treated with LY and incubated for 5 or 30 min. After imaging, the scanned images were projected and the cumulative intensities of the LY signal were measured (Figure 6c and Supporting Information: Figure S8). The results showed that the average LY signal of each glomerulus at 30 min was stronger than that at 5 min (Figure 6c, graph), suggesting that podocytes continuously ingested extracellular solutes. Moreover, we occasionally observed dot-like LY signals in the scanned images, presumably macropinosomes (Supporting Information: Figure S8, enlarged images). Thus, these ex vivo experiments strongly suggest that CDRs form as precursors of macropinocytosis on the surface of isolated glomeruli to ingest extracellular solutes.

Next, we used this technique to determine the locations of the target signals in podocytes ex vivo. After scanning, each layer of the IF images was identified according to its vertical location. As expected, we observed WT1-positive cells at the edges of isolated glomeruli (Figure 6d), indicating that the cells at the edges of the structure were podocytes. Since nephrin and synaptopodin are expressed on the plasma membrane of podocytes for cell-cell interactions called slit diaphragms (Assady et al., 2017; Garg, 2018; L. Liu et al., 2001; Mundel et al., 1997), they can be used to identify the edges of podocytes (Gödel et al., 2011; Inoki et al., 2011; Puelles et al., 2019; Yoshida et al., 2021). Actin and nephrin were detected as ribbon-like pattern representative signals at the slit diaphragms (Figure 6e). Interestingly, we occasionally observed actin-positive but nephrin-negative circular structures, presumably CDRs, at the center of the cells (Figure 6e, arrow). AKT is located at the slit diaphragm (Yu et al., 2018). AKT and synaptopodin double staining indeed revealed colocalization of these proteins in ribbon-like patterns, thus at slit diaphragms (Figure 6f,g and Supporting Information: Figure S7b, SD). We also observed AKT-positive but synaptopodin-negative circular structures in the cells (Figure 6f,g and Supporting Information:

Figure S7b, arrows), suggesting that AKT is located at CDRs in podocytes.

Finally, we treated isolated glomeruli with EIPA to assess the role of CDRs in the AKT signaling pathway in podocytes ex vivo (Figure 7). SEM imaging confirmed that EIPA treatment attenuated CDR formation ex vivo (Figure 7a,b and Supporting Information: Figure S9a). Confocal microscopy imaging showed that the synaptopodin signal was still present as a ribbon-like pattern after the treatment (Figure 7c), suggesting that podocytes on the surface of the isolated glomeruli still functionally maintained the slit diaphragms and that we could exclude toxicity of the drug treatment to interpret the results. The LY assay revealed that the drug treatment also attenuated the ingestion function (Figure 7d,e and Supporting Information: Figure S10). Projection image analysis showed that the total pAKT signal in the glomeruli decreased after EIPA treatment (Figure 7f,g). Notably, we observed actin-positive but synaptopodin-negative circle-like structures (Supporting Information: Figure S9b, arrows), and we detected pAKT signal at the circular actin structures (Supporting Information: Figure S9c), suggesting that AKT was phosphorylated at CDRs. We prepared lysates of the isolated glomeruli after EGF treatment with or without EIPA. Western blot analysis showed that the drug treatment blocked EGF-induced pAKT (Figure 7h). Thus, the results from these EIPA-treatment experiments strongly suggest that CDRs can function as signaling platforms for pAKT in glomerular podocytes ex vivo.

4 | DISCUSSION

In the current study, we observed the formation of CDRs in vivo and clarified their physiological relevance. High-resolution SEM imaging revealed that CDRs formed in glomerular podocytes in vivo (Figure 1), ex vivo (Figures 6a and 7a and Supporting Information: Figure S7a), and in vitro (Figure 3 and Supporting Information: Figure S1), and we visually captured the morphological transition process to macropinocytosis in vitro (Figure 3c,d and Supporting Information: Figure S1c,d) and ex vivo (Figure 6a and Supporting Information: Figure S7a). The results of FDx70 and LY assays confirmed that CDRs underwent macropinocytosis in vitro (Figure 3e-g) and ex vivo (Figure 6c and Supporting Information: Figure S8), respectively. Confocal microscopy showed recruitment of GFP-Btk-PH (Figure 5b and Supporting Information: Figure S5c), GFP-AKT (Supporting Information: Figure S5d), and GFP-mSin1 (Supporting Information: Figure S5e) to CDRs, suggesting the recruitment of AKT and mTORC2 to the plasma membrane via their interaction with PIP3. IF staining for endogenous proteins localized to p110 α (Figure 5a and Supporting Information: Figure S5a), p110 β (Supporting Information: Figure S5b), AKT (Figure 5c and Supporting Information: Figure S6a), pAKT (Figure 5d and Supporting Information: Figure S6b), mTOR (Figure 5e and Supporting Information: Figure S6c), and rictor (Figure 5f and Supporting Information: Figure S6d) in the CDRs. As CDR markers, Rab5a (Lanzetti et al., 2004; A. Palamidessi et al., 2008), SH3YL1 (Hasegawa et al., 2011), and

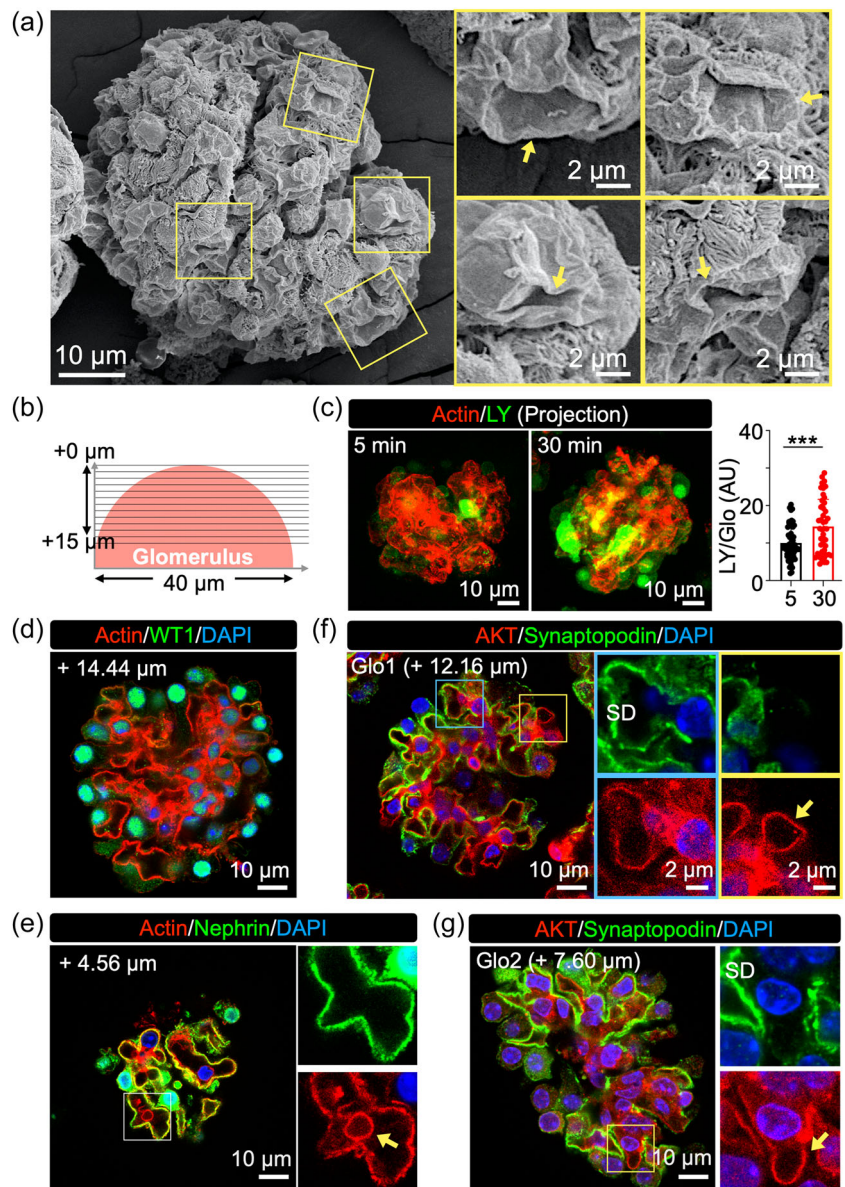


FIGURE 6 Ex vivo experiments revealed AKT recruitment to circular dorsal ruffles (CDRs) expressed in podocytes of isolated glomeruli. (a) Representative high-resolution scanning electron microscope (SEM) images of an isolated glomerulus exhibiting CDR-like structures (squares). Isolated glomeruli were treated with epidermal growth factor (EGF) and fixed for SEM imaging. Structures that resemble the morphological steps of CDR formation in MPC5 cells were identified using high magnification (arrows). $n = 56$ glomeruli from two mice. Scale bars: 10 and 2 μm . (b) Schematic of a method to detect signals from an isolated glomerulus. Images of a glomerulus were scanned along the z-axis from the top as +0 μm at 0.76 μm intervals until the +15 μm section, as illustrated. (c) Representative XY-projection images of actin (red) and Lucifer yellow (LY) (green) staining in an isolated glomerulus. Isolated glomeruli were treated with LY for 5 or 30 min ($n = 17$ or 15 images from three mice, respectively). Scale bar: 10 μm . Graph showing the LY signal inside isolated glomeruli after 5 and 30 min of treatment. *** $p < 0.001$. Two-tailed unpaired Student's t-test was used for the statistical analysis ($n > 40$ glomeruli). (d) Representative confocal image of actin (red) and WT1 (green) staining in an isolated glomerulus. Podocytes identified by WT1 staining were observed at the edge of the glomerulus. $n = 9$ images from three mice. Scale bar: 10 μm . (e) Representative confocal image of actin (red) and nephrin (green) staining in an isolated glomerulus. The CDR was identified as an actin-positive/nephrin-negative ring (arrow in the square). $n = 12$ images from three mice. Scale bar: 10 μm . (f and g) Representative confocal images of AKT (red) and synaptopodin (green) staining in isolated glomeruli (Glo1 and Glo2, respectively) ($n = 26$ images from five mice). Image of Glo3 is shown in Supporting Information: Figure S7b. While AKT was observed at slit diaphragms (SDs in the squares), it was also observed inside the cells as circular structures, presumably CDRs (arrows). Scale bar: 10 μm . The numbers shown in the images indicate the z-axis location of each section (d–g). DAPI, 4', 6-diamidino-2-phenylindole.

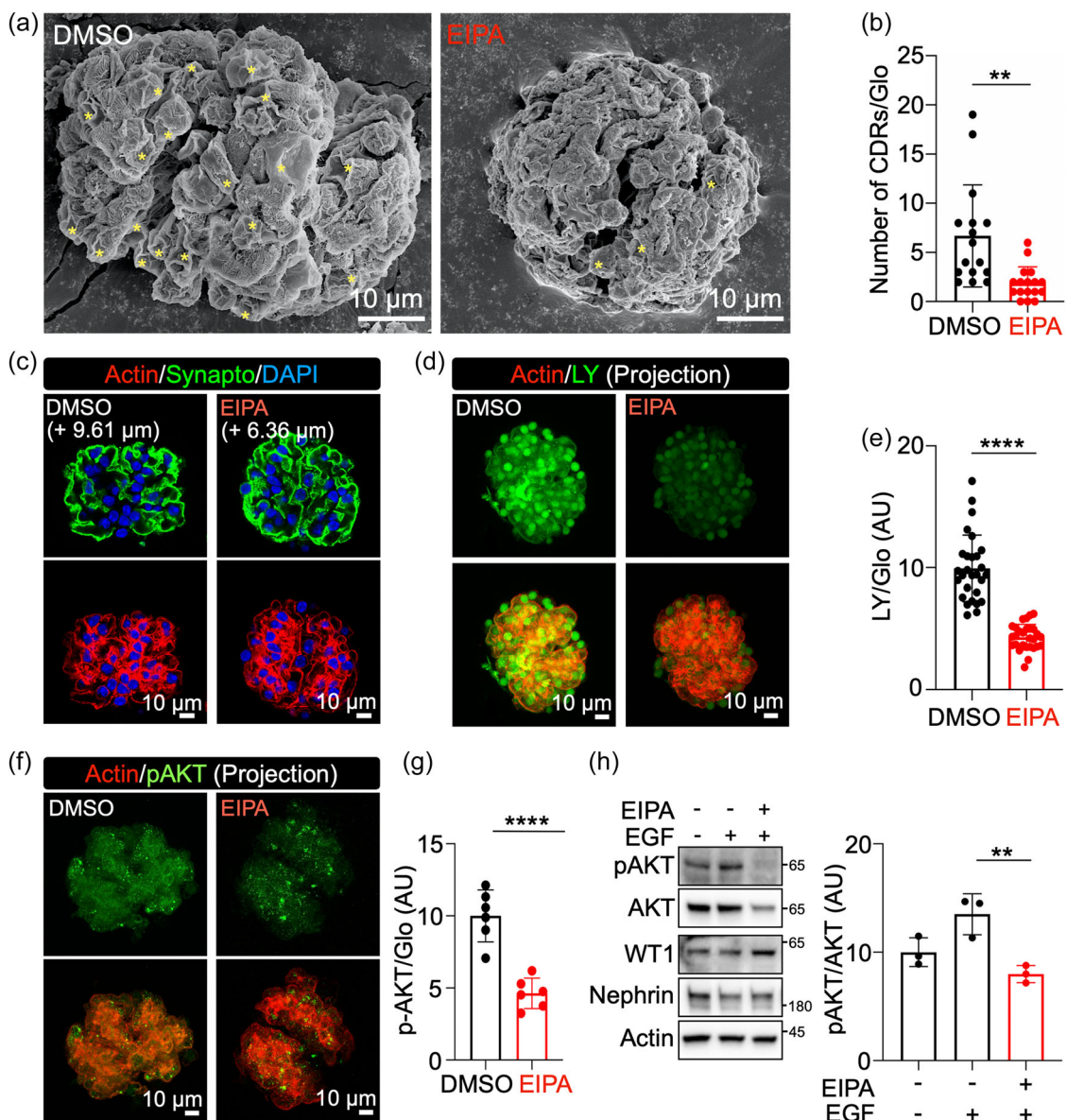


FIGURE 7 5-(N-Ethyl-N-isopropyl)-amiloride (EIPA) treatment attenuated epidermal growth factor (EGF)-induced circular dorsal ruffle (CDR) formation and AKT phosphorylation (pAKT) in glomerular podocytes ex vivo. (a and b) EIPA treatment attenuated CDR formation in glomerular podocytes ex vivo. Representative high-resolution scanning electron microscope (SEM) images of an isolated glomerulus after EGF treatment with and without EIPA (a). The asterisks indicate the locations of CDRs. Additional images are shown in Supporting Information: Figure S9 (a). The graph shows the number of CDRs for each glomerulus, with and without EIPA treatment (b). ** $p < 0.01$. Two-tailed unpaired Student's t-test was used for the statistical analysis. $n = 16$ glomeruli each, from two mice. (c) Representative confocal image of actin (red) and synaptopodin (green) staining in an isolated glomerulus after EGF treatment with and without EIPA. $n = 9$ images each, from two mice. (d and e) EIPA treatment attenuated Lucifer yellow (LY) uptake by glomeruli. Representative XY-projection images of actin (red) and LY (green) staining in an isolated glomerulus after EGF treatment with and without EIPA (d). Graph showing the LY signal of each glomerulus, with and without EIPA treatment (e). **** $p < 0.0001$. Two-tailed unpaired Student's t-test was used for the statistical analysis. $n = 26$ glomeruli each, from two mice. (f and g) EIPA treatment attenuated the cumulative intensities of pAKT signal in a glomerulus. Representative XY-projection images of actin (red) and pAKT (green) staining in an isolated glomerulus after EGF treatment with and without EIPA (f). Graph showing the cumulative intensities of pAKT signal in each glomerulus, with and without EIPA treatment (g). **** $p < 0.0001$. Two-tailed unpaired Student's t-test was used for the statistical analysis. $n = 6$ glomeruli each, from two mice. (h) Western blot analysis of AKT signal from isolated glomeruli after EGF stimulation with and without EIPA. WT1 and nephrin were detected as markers of podocyte. The graph shows the pAKT/AKT ratio for no stimulation, EGF stimulation, and EGF stimulation with EIPA treatment. ** $p < 0.01$. Two-tailed unpaired Student's t-test was used for the statistical analysis ($n = 3$). Scale bar: 10 μm (c, d, and f). AU, arbitrary unit; DMSO, dimethyl sulfoxide.

cortactin (C. L. Cortesio et al., 2010) were also observed (Figure 2b–d). The results of western blot analysis showed that the inhibition of CDRs blocked pAKT in vitro (Figure 4a,b and Supporting Information: Figures S3a,b and S4f–i) and ex vivo (Figure 7h). Thus, we anticipate that GF-induced CDRs may function as signaling platforms for the PI3K/AKT pathway and contribute to the growth, development, and viability of podocytes.

Additionally, the inhibition of CDRs attenuated pS6K (Figure 4a,b and Supporting Information: Figures S3a,b and S4f–i), a well-known mTORC1 substrate. Previous studies have shown that macropinocytosis ingests extracellular nutrients and delivers extracellular amino acids to lysosomes, resulting in mTORC1 activation (Palm et al., 2015; Swanson & Yoshida, 2019; Yoshida et al., 2015). In fact, our data showed that EGF induced pAKT, but not pS6K, under amino acid starvation conditions in vitro (Figure 4e,f and Supporting Information: Figure S3e,f). We also observed that EIPA treatment blocked LY uptake in isolated glomeruli (Figure 7d,e and Supporting Information: Figure S10). It has been shown that mTORC1 is recruited to lysosomes for activation once the concentration of amino acids inside the organelle increase (Condon & Sabatini, 2019; Sancak et al., 2010; Zoncu et al., 2011). Thus, macropinocytosis following CDR formation leads to the ingestion of extracellular nutrients, and the resulting vesicles, macropinosomes, transport them to lysosomes, which would result in the recruitment of mTORC1. Here, we propose a model whereby CDRs promote mTORC1 activity via two mechanisms in podocytes at the surface of glomeruli: (1) CDRs function as a signal platform for the AKT pathway upstream of mTORC1 and (2) CDRs lead to macropinosome formation, which shuttles extracellular nutrients to lysosomes for the mTORC1 recruitment (Figure 8).

The critical role of mTORC1 in podocyte homeostasis has been previously reported. We demonstrated that nondiabetic podocyte-specific TSC1 knockout mice, in which mTORC1 activity in podocytes is constitutively elevated, displayed severe glomerular dysfunction that shared many similar pathological phenotypes with diabetic nephropathy, including mesangial expansion and podocyte loss/detachment, leading to end-stage renal disease by 14 weeks after birth (Inoki et al., 2011). Similarly, genetic ablation of raptor, an essential mTORC1 component in podocytes, causes developmental problems in podocytes and slowly progressive glomerulosclerosis (Gödel et al., 2011). Moreover, several studies have proposed that mTORC1-mediated podocyte hypertrophy is a protective mechanism that preserves glomerular function (Nishizono et al., 2017; Puelles et al., 2019; Zschiedrich et al., 2017). Thus, the appropriate activity of mTORC1 plays a crucial role in maintaining the physiological functions of podocytes (Fantus et al., 2016; Huber et al., 2012). The findings reported here suggest that podocyte CDRs have unique cellular functions that control the mTORC1 pathway.

In summary, through a combination of in vitro, ex vivo, and in vivo experiments, we have identified the expression of CDRs in podocytes and revealed that they function in growth factor signaling. Although the critical roles of mTORC1 in maintaining podocyte viability and function have been well documented, the molecular mechanisms underlying growth factor-induced mTORC1 activity in

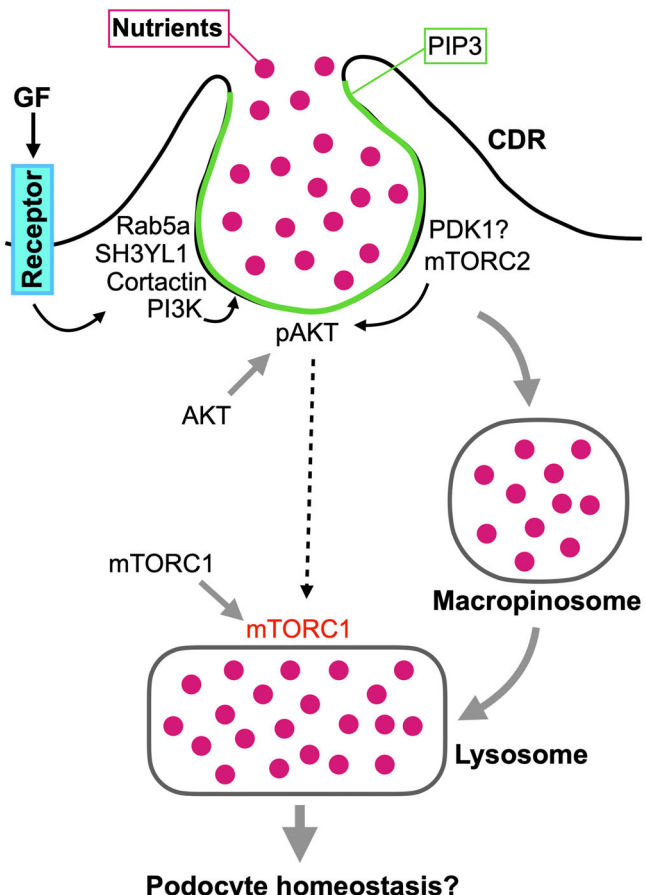


FIGURE 8 Proposed model of the role of circular dorsal ruffles (CDRs) in podocytes. Growth factor (GF) treatment induces CDRs, in which Rab5a, SH3YL1, cortactin, and PI3K are localized. CDR functions as macropinocytosis via the closing process. The resulting vesicles, macropinosomes, deliver extracellular nutrients to the lysosomes, resulting in mTORC1 recruitment. Meanwhile, as the central part of GF signaling pathways, PI3K is activated and synthesizes PIP3 at CDRs; thus, AKT, mTORC2, and, presumably, PDK1, are recruited to the structures. AKT is phosphorylated (pAKT) by mTORC2 and PDK1 at CDRs as the upstream signaling molecule of mTORC1. Since appropriate activation of mTORC1 is critical for podocyte homeostasis, CDR would regulate podocyte functions.

cells have not been well studied. Our observations suggest that CDRs act as key signaling hubs that trigger growth factor-induced mTOR signaling, including both mTORC2 and mTORC1. The findings we report here should shed light on the biological/biochemical research areas of podocytes and provide additional options to target cellular mTOR activity to control mTOR-related kidney diseases.

ACKNOWLEDGMENTS

This study was supported by Frontiers Science Center for Cell Responses Grants from Nankai University (Grant No. C029205001) and the Shenzhen Science and Technology Program (Grant No. JCYJ20210324120813037). We thank Dr. Joel Swanson from the University of Michigan Medical School for reviewing and editing this manuscript.

CONFLICT OF INTEREST STATEMENT

The authors declare no conflict of interest.

ORCID

Sei Yoshida  <http://orcid.org/0000-0002-4771-3900>

REFERENCES

- Assady, S., Wanner, N., Skorecki, K. L., & Huber, T. B. (2017). New insights into podocyte biology in glomerular health and disease. *Journal of the American Society of Nephrology*, 28(6), 1707–1715. <https://doi.org/10.1681/ASN.2017010027>
- Bar-Sagi, D., & Feramisco, J. R. (1986). Induction of membrane ruffling and fluid-phase pinocytosis in quiescent fibroblasts by ras proteins. *Science*, 233(4768), 1061–1068. <https://doi.org/10.1126/science.3090687>
- Bernitt, E., Döbereiner, H. G., Gov, N. S., & Yochelis, A. (2017). Fronts and waves of actin polymerization in a bistability-based mechanism of circular dorsal ruffles. *Nature Communications*, 8, 15863. <https://doi.org/10.1038/ncomms15863>
- Berthiaume, E. P., Medina, C., & Swanson, J. A. (1995). Molecular size-fractionation during endocytosis in macrophages. *Journal of Cell Biology*, 129(4), 989–998. <https://doi.org/10.1083/jcb.129.4.989>
- Bollée, G., Flamant, M., Schordan, S., Fligny, C., Rumpel, E., Milon, M., Schordan, E., Sabaa N., Vandermeersch S., Galaup A., Rodenas A., Casal I., Sunnarborg S. W., Salant D. J., Kopp J. B., Threadgill D. W., Quaggin S. E., Dussaule J. C., Germain S., ... Tharaux P. L. (2011). Epidermal growth factor receptor promotes glomerular injury and renal failure in rapidly progressive crescentic glomerulonephritis. *Nature Medicine*, 17(10), 1242–1250. <https://doi.org/10.1038/nm.2491>
- Buckley, C. M., & King, J. S. (2017). Drinking problems: Mechanisms of macropinosome formation and maturation. *The FEBS Journal*, 284(22), 3778–3790. <https://doi.org/10.1111/febs.14115>
- Chen, J., Zeng, F., Forrester, S. J., Eguchi, S., Zhang, M. Z., & Harris, R. C. (2016). Expression and function of the epidermal growth factor receptor in physiology and disease. *Physiological Reviews*, 96(3), 1025–1069. <https://doi.org/10.1152/physrev.00030.2015>
- Chung, J. J., Huber, T. B., Gödel, M., Jarad, G., Hartleben, B., Kwok, C., Keil, A., Karpitskiy A., Hu J., Huh C. J., Cella M., Gross R. W., Miner J. H., Shaw A. S. (2015). Albumin-associated free fatty acids induce macropinocytosis in podocytes. *Journal of Clinical Investigation*, 125(6), 2307–2316. <https://doi.org/10.1172/JCI79641>
- Commisso, C., Davidson, S. M., Soydaner-Azeloglu, R. G., Parker, S. J., Kamphorst, J. J., Hackett, S., Grabocka, E., Nofal M., Drebin J.A., Thompson C.B., Rabinowitz J.D., Metallo C.M., Vander Heiden M.G., Bar-Sagi D. (2013). Macropinocytosis of protein is an amino acid supply route in Ras-transformed cells. *Nature*, 497(7451), 633–637. <https://doi.org/10.1038/nature12138>
- Condon, K. J., & Sabatini, D. M. (2019). Nutrient regulation of mTORC1 at a glance. *Journal of Cell Science*, 132(21), jcs222570. <https://doi.org/10.1242/jcs.222570>
- Cortesio, C. L., Perrin, B. J., Bennin, D. A., & Huttenlocher, A. (2010). Actin-binding protein-1 interacts with WASp-interacting protein to regulate growth factor-induced dorsal ruffle formation. *Molecular Biology of the Cell*, 21(1), 186–197. <https://doi.org/10.1091/mbc.e09-02-0106>
- Dharmawardhane, S., Schürmann, A., Sells, M. A., Chernoff, J., Schmid, S. L., & Bokoch, G. M. (2000). Regulation of macropinocytosis by p21-activated kinase-1. *Molecular Biology of the Cell*, 11(10), 3341–3352. <https://doi.org/10.1091/mbc.11.10.3341>
- Egami, Y., Taguchi, T., Maekawa, M., Arai, H., & Araki, N. (2014). Small GTPases and phosphoinositides in the regulatory mechanisms of macropinosome formation and maturation. *Frontiers in Physiology*, 5, 374. <https://doi.org/10.3389/fphys.2014.00374>
- Fantus, D., Rogers, N. M., Grahammer, F., Huber, T. B., & Thomson, A. W. (2016). Roles of mTOR complexes in the kidney: Implications for renal disease and transplantation. *Nature Reviews Nephrology*, 12(10), 587–609. <https://doi.org/10.1038/nrneph.2016.108>
- Fu, W., & Hall, M. N. (2020). Regulation of mTORC2 signaling. *Genes*, 11(9), 1045. <https://doi.org/10.3390/genes11091045>
- Garg, P. (2018). A review of podocyte biology. *American Journal of Nephrology*, 47(Suppl 1), 3–13. <https://doi.org/10.1159/000481633>
- Gödel, M., Hartleben, B., Herbach, N., Liu, S., Zschiedrich, S., Lu, S., Debreczeni-Mór, A., Lindenmeyer M. T., Rastaldi M. P., Hartleben G., Wiech T., Fornoni A., Nelson R. G., Kretzler M., Wanke R., Pavenstädt H., Kerjaschki D., Cohen C. D., Hall M. N., ... Huber T. B. (2011). Role of mTOR in podocyte function and diabetic nephropathy in humans and mice. *Journal of Clinical Investigation*, 121(6), 2197–2209. <https://doi.org/10.1172/JCI44774>
- Gu, Z., Noss, E. H., Hsu, V. W., & Brenner, M. B. (2011). Integrins traffic rapidly via circular dorsal ruffles and macropinocytosis during stimulated cell migration. *Journal of Cell Biology*, 193(1), 61–70. <https://doi.org/10.1083/jcb.201007003>
- Guo, J. K. (2002). WT1 is a key regulator of podocyte function: Reduced expression levels cause crescentic glomerulonephritis and mesangial sclerosis. *Human Molecular Genetics*, 11(6), 651–659. <https://doi.org/10.1093/hmg/11.6.651>
- Hasegawa, J., Tokuda, E., Tenno, T., Tsujita, K., Sawai, H., Hiroaki, H., Takenawa, T., Itoh T. (2011). SH3YL1 regulates dorsal ruffle formation by a novel phosphoinositide-binding domain. *Journal of Cell Biology*, 193(5), 901–916. <https://doi.org/10.1083/jcb.201012161>
- Hoon, J. L., Wong, W. K., & Koh, C. G. (2012). Functions and regulation of circular dorsal ruffles. *Molecular and Cellular Biology*, 32(21), 4246–4257. <https://doi.org/10.1128/MCB.00551-12>
- Hoxhaj, G., & Manning, B. D. (2020). The PI3K-AKT network at the interface of oncogenic signalling and cancer metabolism. *Nature Reviews Cancer*, 20(2), 74–88. <https://doi.org/10.1038/s41568-019-0216-7>
- Huber, T. B., Edelstein, C. L., Hartleben, B., Inoki, K., Jiang, M., Koya, D., Kume, S., Lieberthal W., Pallet N., Quiroga A., Ravichandran K., Susztak K., Yoshida S., Dong Z. (2012). Emerging role of autophagy in kidney function, diseases and aging. *Autophagy*, 8(7), 1009–1031. <https://doi.org/10.4161/auto.19821>
- Inoki, K., Li, Y., Xu, T., & Guan, K. L. (2003). Rheb GTPase is a direct target of TSC2 GAP activity and regulates mTOR signaling. *Genes & Development*, 17(15), 1829–1834. <https://doi.org/10.1101/gad.1110003>
- Inoki, K., Mori, H., Wang, J., Suzuki, T., Hong, S., Yoshida, S., Blattner, S. M., Ikenoue T., Ruegg M. A., Hall M. N., Kwiatkowski D. J., Rastaldi M. P., Huber T. B., Kretzler M., Holzman L. B., Wiggins R. C., Guan K. L. (2011). mTORC1 activation in podocytes is a critical step in the development of diabetic nephropathy in mice. *Journal of Clinical Investigation*, 121(6), 2181–2196. <https://doi.org/10.1172/JCI44771>
- Itoh, T., & Hasegawa, J. (2013). Mechanistic insights into the regulation of circular dorsal ruffle formation. *Journal of Biochemistry*, 153(1), 21–29. <https://doi.org/10.1093/jb/mvs138>
- Kay, R. R. (2021). Macropinocytosis: Biology and mechanisms. *Cells & Development*, 168, 203713. <https://doi.org/10.1016/j.cdev.2021.203713>
- Koivusalo, M., Welch, C., Hayashi, H., Scott, C. C., Kim, M., Alexander, T., Touret, N., Hahn K. M., Grinstein S. (2010). Amiloride inhibits macropinocytosis by lowering submembranous pH and preventing Rac1 and Cdc42 signaling. *Journal of Cell Biology*, 188(4), 547–563. <https://doi.org/10.1083/jcb.200908086>

- Kopp, J. B., Anders, H. J., Susztak, K., Podestà, M. A., Remuzzi, G., Hildebrandt, F., & Romagnani, P. (2020). Podocytopathies. *Nature Reviews Disease Primers*, 6(1), 68. <https://doi.org/10.1038/s41572-020-0196-7>
- Lanzetti, L., Palamidessi, A., Areces, L., Scita, G., & Di Fiore, P. P. (2004). Rab5 is a signalling GTPase involved in actin remodelling by receptor tyrosine kinases. *Nature*, 429(6989), 309–314. <https://doi.org/10.1038/nature02542>
- Legg, J. A., Bompard, G., Dawson, J., Morris, H. L., Andrew, N., Cooper, L., Johnston, S. A., Tramontanis, G., Machesky L. M. (2007). N-WASP involvement in dorsal ruffle formation in mouse embryonic fibroblasts. *Molecular Biology of the Cell*, 18(2), 678–687. <https://doi.org/10.1091/mbc.e06-06-0569>
- Liu, G. Y., & Sabatini, D. M. (2020). mTOR at the nexus of nutrition, growth, ageing and disease. *Nature Reviews Molecular Cell Biology*, 21(4), 183–203. <https://doi.org/10.1038/s41580-019-0199-y>
- Liu, L. (2001). Defective nephrin trafficking caused by missense mutations in the NPHS1 gene: Insight into the mechanisms of congenital nephrotic syndrome. *Human Molecular Genetics*, 10(23), 2637–2644. <https://doi.org/10.1093/hmg/10.23.2637>
- Manning, B. D., & Toker, A. (2017). AKT/PKB signaling: Navigating the network. *Cell*, 169(3), 381–405. <https://doi.org/10.1016/j.cell.2017.04.001>
- Mendoza, M. C., Er, E. E., & Blenis, J. (2011). The Ras-ERK and PI3K-mTOR pathways: Cross-talk and compensation. *Trends in Biochemical Sciences*, 36(6), 320–328. <https://doi.org/10.1016/j.tibs.2011.03.006>
- Mundel, P., Heid, H. W., Mundel, T. M., Krüger, M., Reiser, J., & Kriz, W. (1997). Synaptopodin: An actin-associated protein in telencephalic dendrites and renal podocytes. *Journal of Cell Biology*, 139(1), 193–204. <https://doi.org/10.1083/jcb.139.1.193>
- Mundel, P., Reiser, J., Borja, A. Z., Pavenstädt, H., Davidson, G. R., Kriz, W., & Zeller, R. (1997). Rearrangements of the cytoskeleton and cell contacts induce process formation during differentiation of conditionally immortalized mouse podocyte cell lines. *Experimental Cell Research*, 236(1), 248–258. <https://doi.org/10.1006/excr.1997.3739>
- Nishizono, R., Kikuchi, M., Wang, S. Q., Chowdhury, M., Nair, V., Hartman, J., Fukuda, A., Wickman, L., Hodgin, J. B., Bitzer, M., Naik, A., Wiggins, J., Kretzler, M., Wiggins, R. C. (2017). FSGS as an adaptive response to growth-induced podocyte stress. *Journal of the American Society of Nephrology*, 28(10), 2931–2945. <https://doi.org/10.1681/ASN.20170202174>
- Pacitto, R., Gaeta, I., Swanson, J. A., & Yoshida, S. (2017). CXCL12-induced macropinocytosis modulates two distinct pathways to activate mTORC1 in macrophages. *Journal of Leukocyte Biology*, 101(3), 683–692. <https://doi.org/10.1189/jlb.2A0316-141RR>
- Palamidessi, A., Frittoli, E., Garré, M., Faretta, M., Mione, M., Testa, I., Diaspro, A., Lanzetti, L., Scita, G., Di Fiore, P. P. (2008). Endocytic trafficking of Rac is required for the spatial restriction of signaling in cell migration. *Cell*, 134(1), 135–147. <https://doi.org/10.1016/j.cell.2008.05.034>
- Palm, W., Park, Y., Wright, K., Pavlova, N. N., Tuveson, D. A., & Thompson, C. B. (2015). The utilization of extracellular proteins as nutrients is suppressed by mTORC1. *Cell*, 162(2), 259–270. <https://doi.org/10.1016/j.cell.2015.06.017>
- Puelles, V. G., van der Wolde, J. W., Wanner, N., Scheppach, M. W., Cullen-McEwen, L. A., Bork, T., Lindenmeyer, M. T., Gernhold, L., Wong, M. N., Braun, F., Cohen, C. D., Kett, M. M., Kuppe, C., Kramann, R., Saritas, T., van Roeyen, C. R., Moeller, M. J., Tribolet, L., Rebello, R., ... Bertram, J. F. (2019). mTOR-mediated podocyte hypertrophy regulates glomerular integrity in mice and humans. *JCI Insight*, 4(18), e99271. <https://doi.org/10.1172/jci.insight.99271>
- Sancak, Y., Bar-Peled, L., Zoncu, R., Markhard, A. L., Nada, S., & Sabatini, D. M. (2010). Ragulator-Rag complex targets mTORC1 to the lysosomal surface and is necessary for its activation by amino acids. *Cell*, 141(2), 290–303. <https://doi.org/10.1016/j.cell.2010.02.024>
- Schell, C., Baumhakl, L., Salou, S., Conzelmann, A. C., Meyer, C., Helmstädt, M., Wrede, C., Grahammer, F., Eimer, S., Kerjaschki, D., Walz, G., Snapper, S., Huber, T. B. (2013). N-wasp is required for stabilization of podocyte foot processes. *Journal of the American Society of Nephrology*, 24(5), 713–721. <https://doi.org/10.1681/ASN.2012080844>
- Stow, J. L., Hung, Y., & Wall, A. A. (2020). Macropinocytosis: Insights from immunology and cancer. *Current Opinion in Cell Biology*, 35, 131–140. <https://doi.org/10.1016/j.ceb.2020.06.005>
- Sun, X., Liu, Y., Zhou, S., Wang, L., Wei, J., Hua, R., Shen, Z., Yoshida, S. (2022). Circular dorsal ruffles disturb the growth factor-induced PI3K-AKT pathway in hepatocellular carcinoma Hep3B cells. *Cell Communication and Signaling*, 20(1), 102. <https://doi.org/10.1186/s12964-022-00911-6>
- Swanson, J. A. (2008). Shaping cups into phagosomes and macropinosomes. *Nature Reviews Molecular Cell Biology*, 9(8), 639–649. <https://doi.org/10.1038/nrm2447>
- Swanson, J. A., & Watts, C. (1995). Macropinocytosis. *Trends in Cell Biology*, 5(11), 424–428. [https://doi.org/10.1016/s0962-8924\(00\)89101-1](https://doi.org/10.1016/s0962-8924(00)89101-1)
- Swanson, J. A., & Yoshida, S. (2019). Macropinosomes as units of signal transduction. *Philosophical Transactions of the Royal Society B: Biological Sciences*, 374(1765), 20180157. <https://doi.org/10.1098/rstb.2018.0157>
- Thorpe, L. M., Yuzugullu, H., & Zhao, J. J. (2015). PI3K in cancer: Divergent roles of isoforms, modes of activation and therapeutic targeting. *Nature Reviews Cancer*, 15(1), 7–24. <https://doi.org/10.1038/nrc3860>
- Várnai, P., Rother, K. I., & Balla, T. (1999). Phosphatidylinositol 3-kinase-dependent membrane association of the Bruton's tyrosine kinase pleckstrin homology domain visualized in single living cells. *Journal of Biological Chemistry*, 274(16), 10983–10989. <https://doi.org/10.1074/jbc.274.16.10983>
- Wall, A. A., Luo, L., Hung, Y., Tong, S. J., Condon, N. D., Blumenthal, A., Sweet, M. J., Stow, J. L. (2017). Small GTPase Rab8a-recruited phosphatidylinositol 3-kinase γ regulates signaling and cytokine outputs from endosomal toll-like receptors. *Journal of Biological Chemistry*, 292(11), 4411–4422. <https://doi.org/10.1074/jbc.M116.766337>
- Wang, H., Sheng, J., He, H., Chen, X., Li, J., Tan, R., Wang, L., Lan, H. Y. (2019). A simple and highly purified method for isolation of glomeruli from the mouse kidney. *American Journal of Physiology-Renal Physiology*, 317(5), F1217–F1223. <https://doi.org/10.1152/ajprenal.00293.2019>
- West, M. A., Bretscher, M. S., & Watts, C. (1989). Distinct endocytotic pathways in epidermal growth factor-stimulated human carcinoma A431 cells. *J Cell Biol*, 109(6 Pt 1), 2731–2739. <https://doi.org/10.1083/jcb.109.6.2731>
- Ying, H. Z., Chen, Q., Zhang, W. Y., Zhang, H. H., Ma, Y., Zhang, S. Z., Fang, J., Yu, C. H. (2017). PDGF signaling pathway in hepatic fibrosis pathogenesis and therapeutics. *Molecular Medicine Reports*, 16(6), 7879–7889. <https://doi.org/10.3892/mmr.2017.7641>
- Yoshida, S., Hoppe, A. D., Araki, N., & Swanson, J. A. (2009). Sequential signaling in plasma-membrane domains during macropinosome formation in macrophages. *Journal of Cell Science*, 122(Pt 18), 3250–3261. <https://doi.org/10.1242/jcs.053207>
- Yoshida, S., Pacitto, R., Inoki, K., & Swanson, J. (2018). Macropinocytosis, mTORC1 and cellular growth control. *Cellular and Molecular Life Sciences*, 75(7), 1227–1239. <https://doi.org/10.1007/s00018-017-2710-y>
- Yoshida, S., Pacitto, R., Sesi, C., Kotula, L., & Swanson, J. A. (2018). Dorsal ruffles enhance activation of Akt by growth factors. *Journal of Cell Science*, 131(22), jcs220517. <https://doi.org/10.1242/jcs.220517>

- Yoshida, S., Pacitto, R., Yao, Y., Inoki, K., & Swanson, J. A. (2015). Growth factor signaling to mTORC1 by amino acid-laden macropinosomes. *Journal of Cell Biology*, 211(1), 159–172. <https://doi.org/10.1083/jcb.201504097>
- Yoshida, S., Wei, X., Zhang, G., O'Connor, C. L., Torres, M., Zhou, Z., Lin, L., Menon, R., Xu, X., Zheng, W., Xiong, Y., Otto, E., Tang, C. H. A., Hua, R., Verma, R., Mori, H., Zhang, Y., Hu, C. C. A., Liu, M., ... Qi, L. (2021). Endoplasmic reticulum-associated degradation is required for nephrin maturation and kidney glomerular filtration function. *Journal of Clinical Investigation*, 131(7), e143988. <https://doi.org/10.1172/JCI143988>
- Yu, S. M. W., Nissaisorakarn, P., Husain, I., & Jim, B. (2018). Proteinuric kidney diseases: A podocyte's slit diaphragm and cytoskeleton approach. *Frontiers in Medicine*, 5, 221. <https://doi.org/10.3389/fmed.2018.00221>
- Zdżalik-Bielecka, D., Poświata, A., Kozik, K., Jastrzębski, K., Schink, K. O., Brewińska-Olchowik, M., Piwocka, K., Stenmark, H., & Miączyńska, M. (2021). The GAS6-AXL signaling pathway triggers actin remodeling that drives membrane ruffling, macropinocytosis, and cancer-cell invasion. *Proceedings of the National Academy of Sciences of the United States of America*, 118(28), e2024596118. <https://doi.org/10.1073/pnas.2024596118>
- Zobel, M., Disanza, A., Senic-Matuglia, F., Franco, M., Colaluca, I. N., Confalonieri, S., Bisi, S., Barbieri, E., Caldieri, G., Sigismund, S., Pece, S., Chavrier, P., Di Fiore, P. P., & Scita, G. (2018). A NUMB-EFA6B-ARF6 recycling route controls apically restricted cell protrusions and mesenchymal motility. *Journal of Cell Biology*, 217(9), 3161–3182. <https://doi.org/10.1083/jcb.201802023>
- Zoncu, R., Bar-Peled, L., Efeyan, A., Wang, S., Sancak, Y., & Sabatini, D. M. (2011). mTORC1 senses lysosomal amino acids through an inside-out mechanism that requires the vacuolar H(+)-ATPase. *Science*, 334(6056), 678–683. <https://doi.org/10.1126/science.1207056>
- Zschiedrich, S., Bork, T., Liang, W., Wanner, N., Eulenbruch, K., Munder, S., Hartleben, B., Kretz, O., Gerber, S., Simons, M., Viau, A., Burtin, M., Wei, C., Reiser, J., Herbach, N., Rastaldi, M. P., Cohen, C. D., Tharaux, P. L., Terzi, F., ... Huber, T. B. (2017). Targeting mTOR signaling can prevent the progression of FSGS. *Journal of the American Society of Nephrology*, 28(7), 2144–2157. <https://doi.org/10.1681/ASN.2016050519>

SUPPORTING INFORMATION

Additional supporting information can be found online in the Supporting Information section at the end of this article.

How to cite this article: Hua, R., Wei, J., Torres, M., He, Y., Li, Y., Sun, X., Wang, L., Inoki, K., & Yoshida, S. (2023). Identification of circular dorsal ruffles as signal platforms for the AKT pathway in glomerular podocytes. *Journal of Cellular Physiology*, 1–17. <https://doi.org/10.1002/jcp.30996>